aerospace

MDPI

Article

Two-Stage Assumed Mode Method for Flutter Analysis of Supersonic Panels with Elastic Supports and Attached Masses

Wuchao Qi [1,*], Shuai Yuan [1] and Sumei Tian [2]

[1] Key Laboratory of Liaoning Province for Aircraft Composite Structural Analysis and Simulation, Shenyang Aerospace University, Shenyang 110136, China
[2] School of Aeroengine, Shenyang Aerospace University, Shenyang 110136, China; smtian@sau.edu.cn
* Correspondence: qiwuchao@sau.edu.cn

Abstract

During the service life of a supersonic aircraft, panels are susceptible to damaged boundary supports and unexpected attached masses, which can critically alter their flutter characteristics. This paper proposes a novel two-stage assumed mode method to efficiently analyze the modal properties and expanded flutter envelopes of such compromised structures. In the first stage, the bending modes of a Euler–Bernoulli beam under elastic supports in two orthogonal directions are combined to construct the assumed modes of the intact panel, forming a modal matrix that satisfies geometric boundary conditions and establishing the baseline dynamic model. In the second stage, the method is reapplied to derive the generalized eigenvalue problem for the panel with attached masses, accurately capturing the modified mode shapes and frequencies. Subsequently, based on the principle of virtual work and first-order piston theory, the generalized aerodynamic forces are formulated. These are then incorporated into the flutter equations, which are solved in the frequency domain using the p-k method. The results demonstrate that elastic supports generally lower flutter velocities and frequencies. However, an interesting finding is that a centrally attached mass of 0.03 kg (≈10% of the panel mass) can increase the flutter speed by about 10%, whereas the same mass placed off-center may reduce it by roughly 2%. Furthermore, the proposed 9-point damper layout is shown to raise the flutter speed of an elastically supported panel with an off-center mass by up to 18% and the flutter frequency by over 13%, thereby recovering and even exceeding the design flutter boundary.

Keywords: flutter; assumed mode method; panel; elastic support; attached mass

Check for updates

Academic Editors: Enrico Cestino, Giacomo Frulla and Markus Raimund Ritter

Received: 22 November 2025
Revised: 10 January 2026
Accepted: 12 January 2026
Published: 14 January 2026

Copyright: © 2026 by the authors. Licensee MDPI, Basel, Switzerland. This article is an open access article distributed under the terms and conditions of the Creative Commons Attribution (CC BY) license.

1. Introduction

Thin plates are widely employed in aerospace engineering, serving as critical skin components for fuselages and wings [1]. These plates are often subdivided into smaller panels by longitudinal and transverse structural elements, with their boundaries securely fastened to surrounding supports via rivets, adhesives, or other connectors. In the preliminary design phase, panel flutter characteristics are generally analyzed under idealized assumptions of boundary conditions and mass distribution. However, real-world operational environments introduce two significant sources of non-ideality: first, the finite stiffness of supports—which may undergo degradation, loosening, or damage—shifts idealized simple or clamped supports toward more complex elastic restraints; second, attached masses, such as sensors, wiring, ice accumulation, or other on-board equipment, significantly alter the system's mass distribution. The coupled effect of these factors constitutes a complex

dynamic setting that diverges from conventional design assumptions. For instance, in aging aircraft fleets, repeated fatigue loading and environmental corrosion have been reported to loosen or degrade fastener connections, while in-flight ice accretion or retrofitted equipment can introduce substantial unplanned mass—both factors are documented contributors to unexpected aeroelastic responses and have been implicated in several structural-integrity assessments of high-speed flight vehicles. Therefore, investigating the flutter characteristics of panels with elastic supports and attached masses is of considerable practical importance for ensuring flight safety.

Extensive research has been conducted on the dynamic and flutter behaviors of beams and plates under elastic supports. Zhou et al. [2–5] systematically investigated the vibration and thermo-aeroelastic flutter of plate structures under arbitrary boundary conditions. Lin et al. [6] applied the Rayleigh–Ritz method to examine the influence of external stores on the flutter behavior of composite laminates. Su et al. [7] and Tian et al. [8] employed penalty-function-based approaches to analyze the flutter of functionally graded stiffened panels and thin plates with elastic constraints, respectively. While these studies offer valuable insights into the individual effects of elastic supports or attached masses, they do not address the coupled scenario where both factors coexist—a common situation in practical aerospace applications where support degradation and added equipment mass occur simultaneously. This gap limits the ability to accurately predict flutter boundaries in real-world service conditions. Baghaee et al. [9] proposed a novel analytical solution for the flutter of composite plates embedded between two composite layers. Algazin [10] developed an efficient numerical algorithm for studying the flutter of plates with arbitrary planform geometry. These studies collectively confirm that boundary conditions exert a profound influence on the flutter boundaries of panel structures. Jin et al. [11] present a method for examining the free vibration characteristics of multi-span lattice sandwich beams with arbitrary boundary conditions. Xie et al. [12] develop an analytical model for the vibration analysis of L-shaped plates with arbitrary uniform boundary conditions by an artificial spring technique. Sun et al. [13] derive the high-precision closed-form characteristic solutions of the three-dimensional panel flutter problem. They find that boundary conditions could affect the flutter boundary. When the aspect ratio reaches a certain value, the flutter behaviors of three-dimensional panels are similar to those of two-dimensional panels.

Similarly, the influence of attached masses on structural dynamics and aeroelastic behavior has also received significant attention. Fazelzadeh et al. [14,15] used generalized function theory to accurately model the effect of lumped masses attached at arbitrary spanwise and chordwise locations on wings and columns. Peiro' et al. [16] investigated the dynamic response of typical airfoils with emphasis on the role of added mass terms. Wang et al. [17] explored the use of lumped-mass vibration absorbers for suppressing internal resonance in beams. Aydogdu et al. [18] and Rahmane et al. [19] studied the effects of added masses on the free vibration characteristics of composite laminates, with the latter employing the Taguchi method to identify influential parameters. Amoozgar et al. [20] analyzed the aeroelastic stability of a hingeless composite rotor blade with a chordwise-moving mass. Sun et al. [21] and Qi et al. [22] specifically investigated the influence of lumped masses on the supersonic panel flutter using functional gradient design and theoretical modal approaches, respectively. Uymaz [23] examined the vibration of functionally graded plates with temperature-dependent material properties under cantilever boundary conditions. These works consistently demonstrate that attached masses can markedly alter the natural frequencies, mode shapes, and aeroelastic stability of the structure.

Recent advancements continue to expand the toolbox for panel flutter analysis and mitigation. For instance, novel passive suppression techniques such as acoustic black hole

dampers have shown substantial improvements in critical flutter speed [24], while topology-optimized sandwich cores offer a route to extend the flutter-free flight envelope through integrated structural design [25]. Furthermore, extensions of the assumed mode method to advanced composite configurations demonstrate its ongoing applicability for complex panel geometries [26]. Nevertheless, the combined scenario of elastic (damaged) supports and discrete mass attachments—a common real-world condition—remains underexplored in these recent studies, motivating the present integrated two-stage approach.

While existing literature offers valuable insights into the individual effects of elastic supports or attached masses, studies addressing their combined influence remain scarce. In real aerospace applications, however, both factors often coexist, leading to more complex interactions that are not fully captured by isolated models. This gap motivates the present study.

To address this, the present paper develops a two-stage assumed mode method for flutter analysis of supersonic panels under the combined effects of elastic boundary conditions and attached masses. A structural dynamics model is established that incorporates both flexible supports and discrete mass attachments. Generalized aerodynamic forces are derived using first-order piston theory and integrated into the flutter equations, which are solved via the p-k method. Furthermore, this study explores potential strategies for enhancing the flutter speed and frequency through the optimized placement of dampers, providing practical insights for engineering applications.

The present work is motivated by the hypothesis that the combined effect of elastic supports and attached masses—two frequently coexisting yet seldom co-modeled non-ideal factors—can significantly alter the flutter boundary of supersonic panels, and that a structured two-stage assumed-mode approach is capable of efficiently capturing this coupled behavior. Unlike prior studies that have separately addressed elastic boundaries (e.g., Refs. [2–9]) or added masses (e.g., Refs. [14–23]), the proposed method integrates both factors in a unified modal framework. In particular, while recent investigations of mass-attachment effects (e.g., Qi et al. [22]) assumed idealized simply supported boundaries, and analyses of elastic supports typically omit discrete mass terms, the two-stage procedure developed here first constructs the modal basis for the elastically supported panel and then systematically incorporates the inertial contributions of lumped masses. This approach not only generalizes existing formulations but also enables the exploration of novel mitigation strategies, such as optimized damper layouts, to recover or enhance flutter performance under realistic support-and-mass conditions.

2. Geometry of Panels with Damaged Supports and Attached Masses

This study examines a rectangular panel with a uniform cross-sectional thickness, as shown in Figure 1. The panel's longitudinal dimension (along the x-axis, parallel to the fluid flow direction) is denoted as a, its transverse dimension (along the y-axis, perpendicular to the fluid flow) as b, and its depth (along the z-axis, representing the cross-sectional thickness) as h. The outer surface of the panel is exposed to a fluid flow with velocity U_∞, while the inner surface is maintained at ambient static pressure.

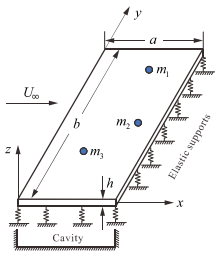


Figure 1. Panels with damaged supports and attached masses.

In traditional panel flutter analysis, simply supported or clamped boundaries on all four sides are often used as idealized boundary conditions. However, the support stiffness in practical engineering structures is finite. Furthermore, during long-term service, connection points (such as rivets or bolts) may experience loosening or damage due to vibrational fatigue, corrosion, or accidental impacts, leading to degradation in boundary support performance. To simulate this real-world "damaged support" condition, this paper employs an elastic support model to more accurately represent the non-ideal characteristics of the boundary conditions, as depicted in Figure 1. To simplify the model while preserving generality, the stiffness of the elastic supports on each side of the panel is assumed to be uniform. The stiffness value can be used to characterize the state of the support, ranging from intact to various degrees of damage.

Additionally, panels in service often carry attached masses such as sensors, wiring, or ice accumulation. These attached masses (shown in Figure 1) alter the system's mass distribution, thereby influencing its dynamic characteristics. Compared to the dimensions of the panel, such attachments can typically be modeled as lumped masses.

In summary, to more accurately predict the flutter characteristics of the panel, the model developed in this study simultaneously accounts for two key non-ideal factors: elastic boundaries simulating damaged supports and attached lumped masses. It is worth noting that the structural modeling approach used in Ref. [22]—where the assumed mode method was applied to a simply supported panel carrying lumped masses—can be regarded as a special case of the present framework when the elastic support stiffness is taken to be infinitely large. The two-stage procedure proposed here, however, is not a direct continuation of that earlier study. Rather, the "first stage" refers to the construction of baseline modes for an elastically supported panel (without masses), and the "second stage" refers to the subsequent incorporation of attached masses into that elastic-panel model. This sequence enables a unified treatment of both damaged (elastic) supports and discrete mass attachments, thereby generalizing the analysis to a broader class of practical configurations.

3. Structural Model via a Two-Stage Assumed Mode Method

3.1. Assumed Modes Formulation for the Elastically Supported Panel

A Euler–Bernoulli beam of uniform cross-section, elastically supported at both ends as illustrated in Figure 2a, is considered. The governing parameters include the beam length l, the mass density ρ, Young's modulus E, the cross-sectional moment of inertia I, and the cross-sectional area S. With the elastic support stiffness coefficients at the two ends denoted as k_1 and k_2, respectively, the objective is to derive the corresponding modes. According to thin plate theory, the transverse bending vibration of a thin panel can be viewed as a two-dimensional extension of the one-dimensional Euler–Bernoulli beam model. For a rectangular panel, when one dimension is significantly larger than the other, the structure can be approximated as a straight beam in the longer direction. More generally, even when the panel dimensions aa and bb are comparable, the vibration modes—particularly in the central region—can be effectively approximated by the product of the beam modes in the two orthogonal directions, as conceptually illustrated in Figure 2b.

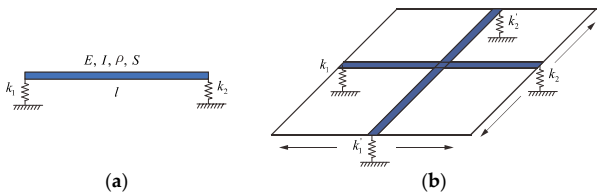


Figure 2. Modes evolution from a beam to a panel with elastic supports: (**a**) A Euler–Bernoulli beam with elastic supports; (**b**) A panel with elastic supports.

Therefore, by introducing the beam-derived mode shape functions $\phi_i(x)$ in the x-direction and $\varphi_j(y)$ in the y-direction, the overall mode shape of the panel without attached masses (as shown in Figure 2b) can be constructed as

$$\psi_{ij}(x,y) = \phi_i(x)\varphi_j(y),\ (i,j = 1,2,3,\ldots) \tag{1}$$

It should be noted that the mode functions $\varphi_j(y)$ along the y-direction also incorporate two elastic support stiffness coefficients. To distinguish them from the coefficients k_1 and k_2 associated with $\phi_i(x)$, the elastic support coefficients in the y-direction are denoted as k_1' and k_2', respectively. Furthermore, when extending the one-dimensional beam mode to the two-dimensional panel, the physical interpretation of these elastic coefficients evolves. They no longer represent discrete end supports but transform into distributed elastic support coefficients, uniformly distributed along the entire panel boundaries, as conceptually illustrated in Figure 2b.

The natural frequencies corresponding to the mode shapes defined in Equation (1) can be calculated and arranged in ascending order, denoted as ω_k. Their corresponding mode shapes are denoted as $\psi_k(x,y)$. In general, the transverse bending displacement $w(x,y,t)$ of the panel can be expressed as a linear combination of these modes

$$w(x,y,t) = \sum_{k=1}^{r} \psi_k(x,y)q_k(t) \tag{2}$$

where r represents the number of truncated modes, and $q_k(t)$ denotes the k-th primary coordinate.

From Equations (1) and (2), it can be inferred that the mode $\psi_k(x,y)$ inherently satisfies the elastic support boundary conditions on all four sides of the panel. When extending the analysis to a panel with several lumped masses, these modes can be adopted as the assumed modes that satisfy the geometric (displacement) boundary conditions. The presence of attached masses will be accounted for in the subsequent formulation of the system's energy expressions, particularly the kinetic energy, thereby enabling the derivation of the modified structural matrices for the generalized eigenvalue problem.

3.2. Generalized Eigenvalue Problem Incorporating Attached Masses

Accounting for the large-displacement and small-strain postulate proposed by von Kármán but neglecting in-plane tensile deformations, the elastic potential energy of the panel shown in Figure 2b is given by

$$U = \frac{D_b}{2}\iint \left[\left(\frac{\partial^2 w}{\partial x^2}\right)^2 + \left(\frac{\partial^2 w}{\partial y^2}\right)^2 + 2\mu\frac{\partial^2 w}{\partial x^2}\frac{\partial^2 w}{\partial y^2} + 2(1-\mu)\left(\frac{\partial^2 w}{\partial x \partial y}\right)^2 \right] \mathrm{d}x\mathrm{d}y \tag{3}$$

where μ is the Poisson's ratio, $D_b = Eh^3/12(1-\mu^2)$ is the bending stiffness and h is the thickness of the panel.

When N_p lumped masses are attached to the panel, the total kinetic energy T of the system is the sum of the panel's transverse bending kinetic energy T_b and the kinetic energy T_a of the attached masses, expressed as

$$T = T_b + T_a = \frac{1}{2}\iint \overline{m}\left(\frac{\partial w}{\partial t}\right)^2 \mathrm{d}x\mathrm{d}y + \frac{1}{2}\sum_{p=1}^{N_p} m_p \left[\frac{\partial w(x_p, y_p)}{\partial t}\right]^2 \tag{4}$$

where $\overline{m}$ signifies the mass per unit area of the panel, x_p and y_p denote the x-coordinate and y-coordinate, respectively, of the p-th mass attachment.

Substituting the transverse bending displacement Equation (2) based on the assumed modal expression into Equation (3), the expression of the bending potential energy of the panel becomes

$$U = \frac{1}{2}\sum_{m=1}^{r}\sum_{n=1}^{r}\widetilde{k}_{mn}q_m(t)q_n(t),\ (m,n=1,2,\ldots r) \tag{5}$$

where

$$\widetilde{k}_{mn} = D_b\iint\left[\frac{\partial^2\psi_m}{\partial x^2}\frac{\partial^2\psi_n}{\partial x^2} + \frac{\partial^2\psi_m}{\partial y^2}\frac{\partial^2\psi_n}{\partial y^2} + 2\mu\frac{\partial^2\psi_m}{\partial x^2}\frac{\partial^2\psi_n}{\partial y^2} + 2(1-\mu)\frac{\partial^2\psi_m}{\partial x\partial y}\frac{\partial^2\psi_n}{\partial x\partial y}\right]\mathrm{d}x\mathrm{d}y \tag{6}$$

Similarly, substituting Equation (2) into Equation (4), the overall kinetic energy can be expressed as follows

$$T = \frac{1}{2}\sum_{m=1}^{r}\sum_{n=1}^{r}\widetilde{m}_{mn}\dot{q}_m(t)\dot{q}_n(t) \tag{7}$$

where

$$\widetilde{m}_{mn} = \rho h\iint\psi_m(x,y)\psi_n(x,y)\mathrm{d}x\mathrm{d}y + \sum_{p=1}^{N_p}m_p\psi_m(x_p,y_p)\psi_n(x_p,y_p) \tag{8}$$

Let $\widetilde{\boldsymbol{K}} = \left[\widetilde{k}_{mn}\right]_{r\times r}$ and $\widetilde{\boldsymbol{M}} = [\widetilde{m}_{mn}]_{r\times r}$, and address the generalized eigenvalue problem

$$\left|\widetilde{\boldsymbol{K}} - \widetilde{\omega}^2\widetilde{\boldsymbol{M}}\right| = 0 \tag{9}$$

Subsequently, the first s-th natural frequencies and eigenvectors of the system equipped with mass attachments can be determined as $\widetilde{\omega}_s$, $(k=1,\ldots,s)$ and $\boldsymbol{a}_1,\ldots,\boldsymbol{a}_s$, respectively. Furthermore, let $\boldsymbol{\Phi} = [a_1,\ldots,a_s]_{r\times s}$, $\overline{\boldsymbol{\psi}} = [\overline{\psi}_1,\ldots,\overline{\psi}_s]$ and $\boldsymbol{\psi} = [\psi_1,\ldots,\psi_r]$, the correlation between the assumed modes and the approximate modes of the panel equipped with mass attachments is as follows

$$\overline{\boldsymbol{\psi}} = \boldsymbol{\psi}\boldsymbol{\Phi} \tag{10}$$

Therefore, the m-th mode is

$$\overline{\psi}_m(x,y) = \sum_{n=1}^{r}\psi_n(x,y)a_{nm},\ (m=1,2,\ldots s,\ n=1,2,\ldots r) \tag{11}$$

Then the transvers displacement function $w(x,y,t)$ of the panel with elastic supports and mass attachments can be expressed as

$$w(x,y,t) = \sum_{m=1}^{s}\overline{\psi}_m(x,y)q_m(t) = \sum_{m=1}^{s}\sum_{n=1}^{r}\psi_n(x,y)a_{nm}q_m(t) \tag{12}$$

3.3. Dynamic Equations

By introducing the primary mass parameter

$$M_m = \iint\overline{m}\left[\overline{\psi}_m(x,y)\right]^2\mathrm{d}x\mathrm{d}y \tag{13}$$

and the primary stiffness parameter

$$K_m = D_b\iint\left[\frac{\partial^2\psi_m}{\partial x^2}\frac{\partial^2\psi_m}{\partial x^2} + \frac{\partial^2\psi_{mi}}{\partial y^2}\frac{\partial^2\psi_m}{\partial y^2} + 2\mu\frac{\partial^2\psi_m}{\partial x^2}\frac{\partial^2\psi_m}{\partial y^2} + 2(1-\mu)\frac{\partial^2\psi_m}{\partial x\partial y}\frac{\partial^2\psi_{mi}}{\partial x\partial y}\right]\mathrm{d}x\mathrm{d}y \tag{14}$$

the first r natural frequencies of the panel are

$$\overline{\omega}_m = \sqrt{\frac{K_m}{M_m}}, m = 1, 2, \ldots, r. \tag{15}$$

Additionally, the mass matrix and stiffness matrix can be expressed as $\boldsymbol{M} = [M_m]_{r\times r}$ and $\boldsymbol{K} = [K_m]_{r\times r}$, respectively. Thus the system motion equation represented by the modal coordinate can be obtained as

$$M_m\ddot{q}_m(t) + C_m\dot{q}_m(t) + K_m q_m(t) = Q_m(t),\ (m = 1, 2, \ldots, r) \tag{16}$$

where C_m and $Q_m(t)$ are the m-th modal damping coefficient and the m-th modal aerodynamic force, which will be established in the next section.

4. Flutter Analysis

4.1. Formulation of Generalized Aerodynamic Forces

When the outer surface of the elastically supported panel with mass attachments is subjected to a supersonic airflow, the resulting pressure difference across the panel, according to the first-order piston theory, is given by

$$\Delta p(x, y, t) = -\frac{2q_d}{Ma_\infty}\left(\frac{\partial w(x, y, t)}{\partial x} + \frac{1}{U_\infty}\frac{\partial w(x, y, t)}{\partial t}\right) \tag{17}$$

where q_d stands for the dynamic pressure and Ma_∞ represents the Mach number of undisturbed air. The explicit form of the aerodynamic pressure difference according to first-order piston theory is given in Equation (17). The subsequent steps for incorporating this pressure into the modal equations of motion, leading to the final coupled aeroelastic system. Substitute Equation (12) into Equation (17), we can rephrase the pressure difference $\Delta p(x, y, t)$ as

$$\Delta p(x, y, t) = -\frac{2q_d}{Ma_\infty}\left(\sum_{m=1}^{r}\sum_{n=1}^{r}\frac{\partial \psi_n(x, y)}{\partial x}a_{nm}q_m(t) + \frac{1}{U_\infty}\sum_{m=1}^{r}\sum_{n=1}^{r}\psi_n(x, y)a_{nm}\dot{q}_m(t)\right) \tag{18}$$

Consequently, the m-th modal aerodynamic force Q_m can be expressed as

$$Q_m = \iint \Delta p(x, y, t)\psi_m(x, y)\mathrm{d}x\mathrm{d}y = -\frac{2q_d}{Ma_\infty}\sum_{n=1}^{r}\left(\overline{D}_{mn}q_n(t) + \frac{1}{U_\infty}\overline{E}_{mn}\dot{q}_n(t)\right) \tag{19}$$

where

$$\overline{D}_{mn} = \iint\left[\left(\sum_{s=1}^{r}\psi_s(x, y)a_{sm}\right)\left(\sum_{s=1}^{r}\frac{\partial \psi_s(x, y)}{\partial x}a_{sn}\right)\right]\mathrm{d}x\mathrm{d}y \tag{20}$$

$$\overline{E}_{mn} = \iint\left[\left(\sum_{s=1}^{r}\psi_s(x, y)a_{sm}\right)\left(\sum_{s=1}^{r}\psi_s(x, y)a_{sn}\right)\right]\mathrm{d}x\mathrm{d}y \tag{21}$$

Equation (19) reveals that the coefficient $\overline{D}_{mn}$ associated with $q_n(t)$ embodies the aerodynamic stiffness, while the coefficient $\overline{E}_{mn}$ linked to $\dot{q}_n(t)$ represents the aerodynamic damping.

4.2. p-k Method for Flutter Calculation

Substituting Equation (19) into Equation (16), the aeroelastic equation of the panel equipped with elastic supports and mass attachments can be expressed in the modal coordinate system as

$$M_m\ddot{q}_m + C_m\dot{q}_m + K_m q_m = -\frac{2q_d}{Ma_\infty}\sum_{n=1}^{r}\left(\overline{D}_{mn}q_n(t) + \frac{1}{U_\infty}\overline{E}_{mn}\dot{q}_n(t)\right),\ (m = 1, 2, \ldots, r) \tag{22}$$

Equation (22) can be reformulated as

$$\boldsymbol{M}\ddot{\boldsymbol{q}}(t) + \boldsymbol{C}\dot{\boldsymbol{q}}(t) + \boldsymbol{K}\boldsymbol{q}(t) = -\frac{2q_d}{Ma_\infty}\left(\overline{\boldsymbol{D}}\boldsymbol{q}(t) + \frac{1}{U_\infty}\overline{\boldsymbol{E}}\dot{\boldsymbol{q}}(t)\right) \tag{23}$$

Equation (23) constitutes the time-domain representation of the flutter equation for the panel with elastic supports and mass attachments, as inferred from the 1-st order piston theory. To ascertain the flutter characteristics of the panel, the *p*-*k* method will be employed to obtain insights, such as the flutter speed, flutter frequency, and the suddenness of the system's transition into the flutter state. For this purpose, we reformulate the modal displacement $\boldsymbol{q}(t)$ of the system as

$$\boldsymbol{q}(t) = \overline{\boldsymbol{q}}e^{st} \tag{24}$$

where $\overline{\boldsymbol{q}}$ denotes the amplitude of $\boldsymbol{q}(t)$, $s = (\gamma + \mathrm{i})\omega$ and γ is the transient decay rate coefficient. Introducing a dimensionless parameter

$$p = (\gamma + 1)k_R \tag{25}$$

where k_R is the reduced frequency. Then Equation (24) can be rewritten as

$$\boldsymbol{q}(t) = \overline{\boldsymbol{q}}e^{2pU_\infty t/a} \tag{26}$$

By substituting Equation (26) into Equation (23), we derive the quadratic eigenvalue problem for the aeroelastic system of the panel with elastic supports and mass attachments, expressed as follows

$$\left[\overline{\boldsymbol{A}}p^2 + \overline{\boldsymbol{B}}p + \overline{\boldsymbol{C}}\right]\overline{\boldsymbol{q}} = 0 \tag{27}$$

where

$$\overline{\boldsymbol{A}} = \left(\frac{2U_\infty}{a}\right)^2\boldsymbol{M} \tag{28}$$

$$\overline{\boldsymbol{B}} = \frac{2U_\infty}{a}\boldsymbol{C} - q_d\frac{\boldsymbol{Q}_{\mathrm{Im}}(k_R, Ma_\infty)}{k_R} \tag{29}$$

$$\overline{\boldsymbol{C}} = \boldsymbol{K} - q_d\boldsymbol{Q}_{\mathrm{Re}}(k_R, Ma_\infty) \tag{30}$$

and $\boldsymbol{Q}(k_R, Ma_\infty) = -\frac{2}{Ma_\infty}\left(\overline{\boldsymbol{D}} + \frac{2p}{a}\overline{\boldsymbol{E}}\right)$.

Due to the fact that $p = (\gamma + \mathrm{i})k_R$, and the system matrix are the functions of k_R, the calculation of p needs to be performed iteratively. When convergence is achieved at the current flow velocity U_∞, the values of structural damping g and frequency f(Hz) can be determined as

$$g \approx 2\gamma = 2\frac{\mathrm{Re}(p)}{k_R} \tag{31}$$

$$f = \frac{k_R U_\infty}{a\pi} \tag{32}$$

Based on the modeling and analysis framework established above, and to clearly illustrate the overall technical approach and parametric study structure of this research, Figure 3 presents the computational flow and case planning of the proposed two-stage assumed mode method and the subsequent flutter analysis. This flowchart systematically outlines the entire process, from the structural dynamics modeling of elastic supports and attached masses to aerodynamic modeling and flutter solution via the *p*-*k* method, and categorically lists the parametric cases investigated, including support conditions, mass configurations, and damper layouts. In the following sections, numerical examples will be systematically computed and discussed based on this analytical framework for each working condition.

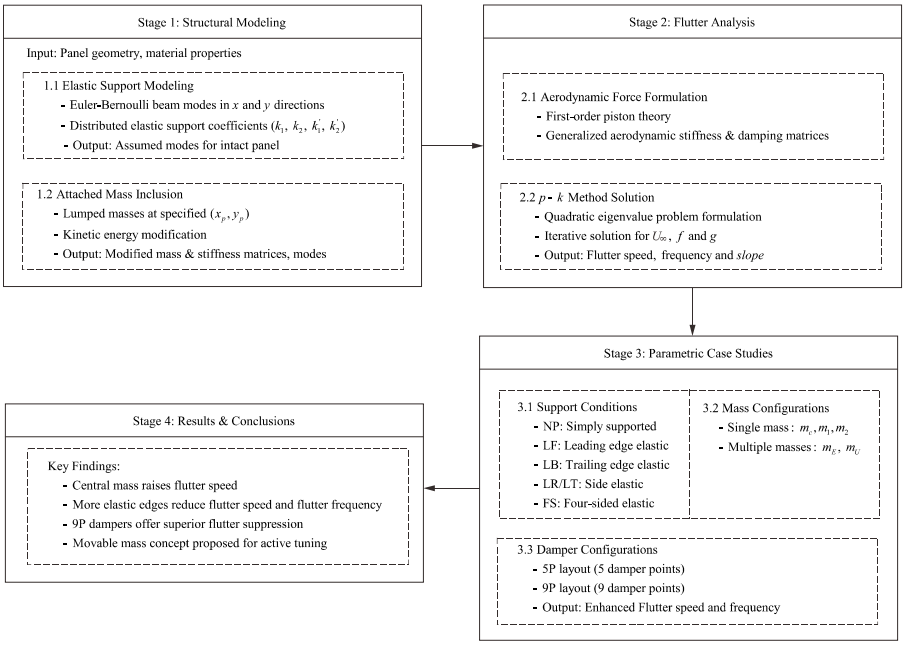


Figure 3. A panel designed for supersonic flight.

5. Numerical Examples

Figure 4a displays a panel designed for supersonic flight. Its side lengths are $a = b = 0.3$ m, and its thickness is 0.0012 m. These dimensions are representative of typical panel sizes encountered in the skin structures of supersonic aircraft wings and fuselage sections, where panel aspect ratios near unity and thicknesses on the order of 1 mm are common for lightweight design. For instance, similar dimensions have been adopted in benchmark studies on supersonic panel flutter and are consistent with the scale of structural panels in high-speed flight vehicles (see, e.g., Refs. [9,22]). The panel is crafted from high-strength aluminum alloy, and its physical parameters are outlined in Table 1 [27].

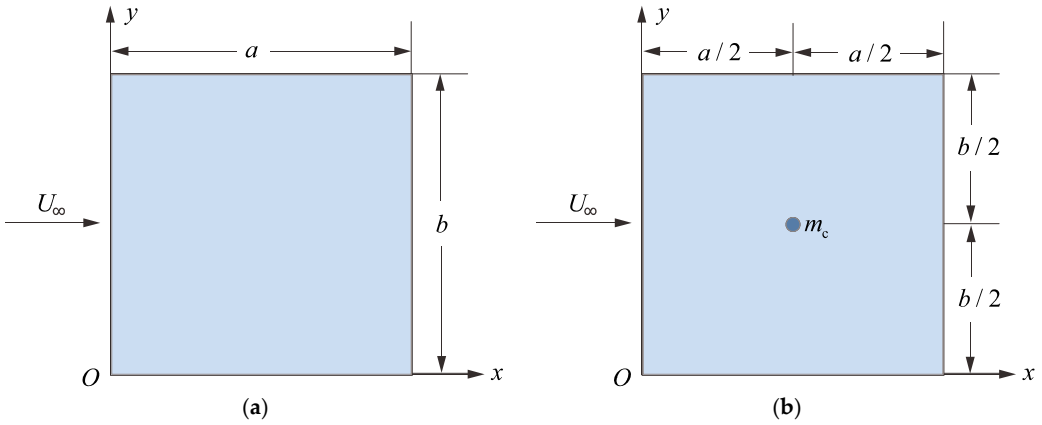


Figure 4. A panel designed for supersonic flight: (**a**) in the absence of mass attachments; (**b**) with a mass attachment m_c located at the center of the panel.

Table 1. Physical parameters of the panel.

Physical Parameter	Value
Young's modulus (Pa)	$E = 7.1 \times 10^{10}$
Poisson's ratio	$v = 0.32$
Mass density (kg/m^3)	$\rho_s = 2768$
Modal damping ratio (%)	$\zeta = 0.0$

The ideal case of a simply supported panel without added masses serves as a baseline, with its natural frequency given by the analytical solution

$$\omega_{ij} = \pi^2 \left(\frac{i^2}{a^2} + \frac{j^2}{b^2} \right) \sqrt{\frac{D_b}{\rho_s h}} (i, j = 1, 2, \ldots) \tag{33}$$

For the elastically supported panel in Figure 4a, its dynamic properties should converge to this baseline as the support stiffness increases—a key physical insight used to verify the proposed method. Table 2 quantifies this convergence trend by listing the first six natural frequencies under varying stiffness coefficients, thereby confirming the precision of our modal algorithm.

Table 2. Variation in the first six natural frequencies of the panel with the stiffness coefficient of the elastic supports.

k ($\times 10^6$ N/m^2)	f_1 (Hz)	f_2 (Hz)	f_3 (Hz)	f_4 (Hz)	f_5 (Hz)	f_6 (Hz)
0.1	50.57	107.29	107.29	147.22	163.96	163.96
0.5	60.01	143.32	143.32	212.05	262.89	262.89
1.0	61.95	151.14	151.14	230.07	290.28	290.28
3.0	63.48	157.35	157.35	246.22	310.45	310.45
5.0	63.83	158.75	158.75	250.09	314.86	314.86
7.0	63.99	159.37	159.37	251.83	317.37	317.37
9.0	64.08	159.73	159.73	252.84	318.42	318.42
11.0	64.15	159.96	159.96	253.49	319.09	319.09
Inf	64.64	161.60	161.60	258.56	323.20	323.20

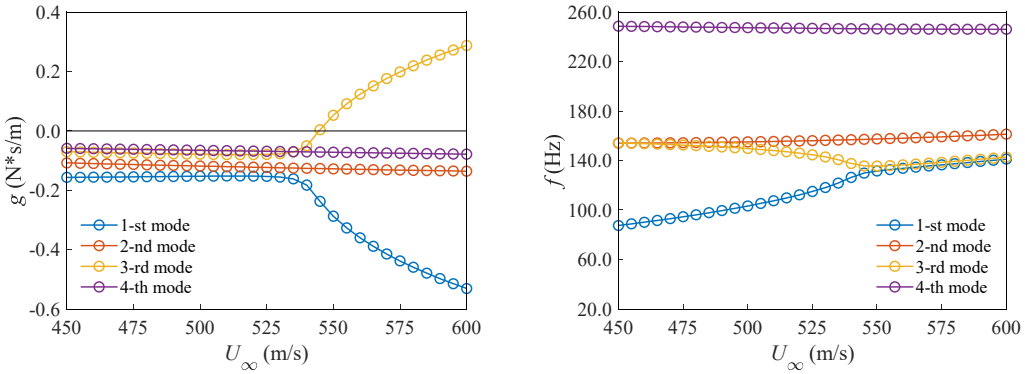
As observed in Table 2, the first six natural frequencies of the panel consistently converge to the benchmark values of the simply supported case as the distributed spring stiffness coefficient increases. This trend provides clear validation for the accuracy of the proposed algorithm in calculating the modal characteristics of elastically supported panels. It is noteworthy that at relatively low stiffness coefficients (e.g., $k = 0.1 \times 10^6$ N/m^2), significant deviations from the simply supported benchmark occur. For instance, the sixth-order natural frequency exhibits a maximum discrepancy of 49.27%. This substantial deviation underscores the considerable influence of boundary stiffness on panel dynamics, particularly for higher-order modes. More importantly, these findings highlight the critical necessity of accounting for elastic supports in panel flutter analysis. Relying on idealized simply supported boundary conditions may lead to non-conservative or inaccurate flutter predictions, whereas the present methodology enables a more realistic and reliable assessment.

As a benchmark, flutter analysis of the four-sided simply supported panel is first performed using the *p*-*k* method. The first 16 structural modes (i.e., $i, j = 4$ in Equation (1)) are included in the simulation, while structural damping is neglected. The assumption of zero structural damping provides a conservative baseline (lowest flutter speed). In practice, inherent material and joint damping (typically $\zeta < 0.5\%$ for metallic aircraft panels) would raise the flutter velocity slightly. For example, a 0.5% modal damping ratio could increase the flutter speed of the simply supported panel by approximately 1–2%. This level of variation does not affect the comparative trends observed across the different support and mass configurations, which are the primary focus of this study. The air density is set to $\rho_\infty = 1.226$ kg/m^3, and the mass ratio is taken as $\rho_r = 1.0$. The variation in the modal damping with velocity is illustrated in Figure 5.

Figure 5 shows that the flutter velocity and frequency for the simply supported case are $U_F = 544.67$ m/s and $f_F = 135.77$ Hz, respectively, with flutter occurring in the 3rd mode. For the simply supported rectangular panel, the third mode corresponds to the (2,1) plate-bending mode (two half-waves along the flow direction, one half-wave across the span). A detailed visualization of this mode shape and its role in the coupled flutter mechanism can be found in Ref. [22]. It is apparent from Figure 5b that the 1st and 3rd modes coalesce during the flutter. In a simply supported rectangular panel, the first mode (1,1) and the third mode (2,1) share a similar transverse (span-wise) symmetry, but differ in the number of half-waves along the streamwise direction. Under first-order piston theory, the aerodynamic stiffness term is proportional to the streamwise slope of the mode shape. The (2,1) mode has a higher streamwise curvature and thus experiences stronger aerodynamic

stiffening as velocity increases. Meanwhile, the (1,1) mode is more sensitive to inertial and stiffness effects. At a critical velocity, the natural frequencies of these two modes approach each other, and the aerodynamic damping (which is velocity-dependent) can no longer dissipate the energy exchanged between them, leading to frequency coalescence and flutter onset.

Furthermore, the slope of the 3rd mode curve at $U_F = 544.67$ in Figure 5a can be used as a criterion to evaluate the abruptness of the flutter onset. This index, termed the flutter slope, is denoted as s_F. Based on the slope of the curve, we obtain $s_F = 0.0108$.



(**a**) (**b**)

Figure 5. Results of flutter calculation for the panel under simply supported conditions on four sides (NP): (**a**) $U - g$; (**b**) $U - f$.

For comparison, the same case is analyzed using the Nastran software v2020 (*p-k* method), which yields $U_F = 541.2$ m/s and $f_F = 133.5$ Hz [9]. The relative errors between the two methods are 0.32% in flutter speed and 1.70% in flutter frequency, confirming the accuracy of the present approach. The excellent agreement with both an independent commercial solver (Nastran) and the published results of Ref. [9] confirms that the present model meets established benchmark standards for simply supported panel flutter prediction. For subsequent discussion, the case of a simply supported panel with no mass attachments is designated as NP.

Next, we consider the cases where there is only one mass attached to the panel. This problem is investigated under different elastic boundary conditions and is divided into three subsections. Section 5.1 discusses the case where only one side of the panel is elastically supported, which is further divided into four sub-cases. Section 5.2 considers the case where all four sides of the panel are elastically supported. The scenario with more than one mass attachment will be discussed in Section 5.3. Furthermore, in Section 5.4, we present two different damper configurations and discuss their effectiveness in suppressing panel flutter.

5.1. Flutter Calculation of the Panel with Single-Sided Elastic Supports

When only one side of the panel is elastically supported, the support coefficients for the remaining three sides are assigned a sufficiently large value (e.g., 1×10^{10} N/m^2, which has been verified as adequately rigid based on the convergence study in Table 2). Depending on the location of the elastic support relative to the supersonic flow direction, three representative configurations are defined: Case LF, where the leading (front) edge is elastically supported; Case LB, where the leeward (back) edge is elastically supported; and Cases LR/LT, where either the left (root) or the right (tip) side is elastically supported, respectively.

The effect of attached masses on the panel's mode shapes has been systematically investigated in earlier work (see, e.g., ref. [22], where the Modal Assurance Criterion (MAC) was employed to quantify mode-shape correlation). In line with those findings, a centrally placed mass (m_c) predominantly affects the symmetric low-order modes, stiffening the fundamental mode and thereby raising the flutter speed. Off-center masses (m_1 and m_2), in contrast, break symmetry and strengthen coupling between the first and second bending modes, which promotes earlier flutter onset. Since the detailed mode-shape analysis has already been reported, the present study focuses on the resulting flutter characteristics (speed, frequency and onset abruptness) within the proposed two-stage assumed-mode framework.

5.1.1. The Case of LF

The elastic support stiffness coefficient is set to 1×10^6 N/m^2, and a lumped mass of 0.03 kg, representing approximately 10% of the panel's total mass, is attached at the panel center, as shown in Figure 4b. The corresponding flutter characteristics computed by the proposed algorithm at $Ma_\infty = 2.0$ are summarized in Figure 6.

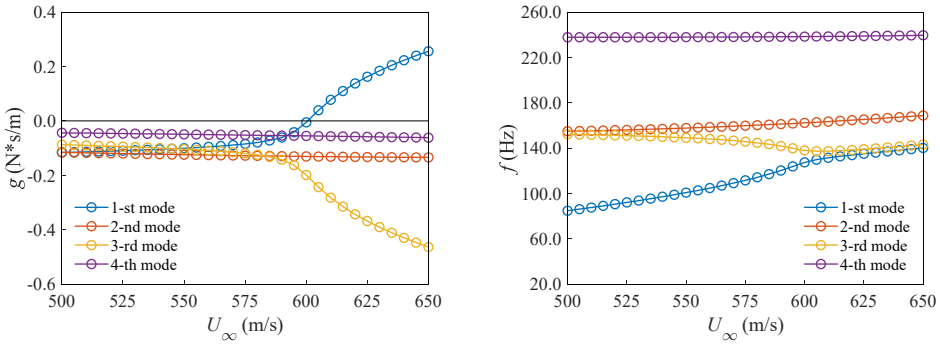


Figure 6. Flutter analysis results (LF-m_c) ($Ma_\infty = 2.0$): (**a**) $U - g$; (**b**) $U - f$.

As illustrated in Figure 6, for the LF configuration with the central mass attachment, the panel exhibits a flutter speed of 600.57 m/s, a flutter frequency of 127.72 Hz, and a suddenness factor of 0.0089. Flutter occurs in the first mode, driven by coupling between the first and third modes. Compared to the baseline simply supported panel without mass (Figure 5), the flutter speed increases by approximately 10.26%, while the flutter frequency decreases by about 5.93%. Given these results, it remains challenging to attribute the increase in flutter speed to a single factor. To further elucidate the individual contributions of elastic support stiffness and added mass, we systematically vary each parameter independently while holding the other constant. Specifically, the stiffness coefficient k of the elastic support and m_c of the centrally located mass are adjusted separately to observe their respective influences on the flutter characteristics. The resulting variations are presented in Figure 7.

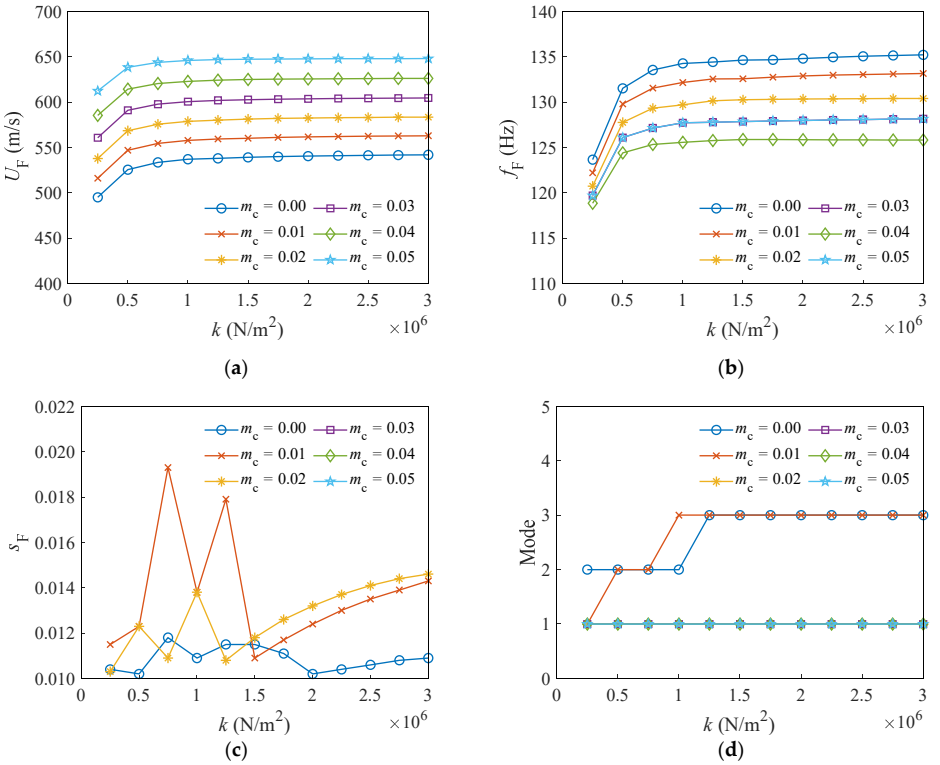


Figure 7. Flutter characteristics vs. the stiffness coefficient of the elastic support for different mass: (**a**) Flutter speeds; (**b**) flutter frequencies; (**c**) Flutter slopes; (**d**) flutter modes.

As shown in Figure 7a, attaching a mass at the panel center effectively increases the flutter speed of the elastically supported panel. This improvement is monotonic: the larger the mass m_c, the higher the resulting flutter speed. Specifically, compared to the case without added mass, attaching a 0.03 kg mass increases the flutter speed by approximately 11.56%, while a 0.05 kg mass raises it by about 19.59%. When m_c is held constant, the flutter speed also increases monotonically with the elastic support stiffness coefficient k, though the rate of increase diminishes at higher stiffness values, indicating a convergent trend. Figure 7b reveals that for a constant m_c, the flutter frequency also exhibits a monotonic and convergent trend as the support stiffness increases. Moreover, for $m_c < 0.04$ kg, the flutter frequency gradually decreases with increasing mass. However, when $m_c = 0.05$ kg, the flutter frequency returns to a level similar to that observed at $m_c = 0.03$ kg. The abruptness of the flutter onset is illustrated in Figure 7c. The suddenness factor s_F remains relatively low in most cases, except for two distinct extreme points observed at $m_c = 0.01$ kg. Figure 7d indicates that for small attached masses, the flutter mode alternates between the second and third modes. As the mass increases, however, flutter predominantly occurs in the first mode.

In summary, attaching a mass at the panel center can effectively enhance the flutter speed of an elastically supported panel, albeit with a slight reduction in flutter frequency. This finding leads to a subsequent question: how do the flutter characteristics change when the attachment position is varied? To address this, we relocate the mass from the center to two other positions: the point at 1/2 span and 1/4 chord (Figure 8a), and the point at 1/4 span and 1/4 chord (Figure 8b). The masses at these positions are denoted as m_1 and m_2, respectively, as illustrated in Figure 8.

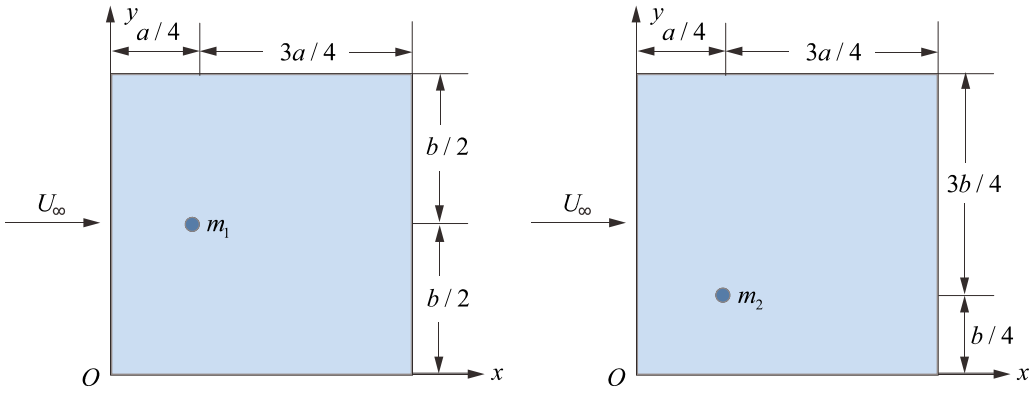


Figure 8. Two distinct locations for the mass attachment are considered: (**a**) The intersection point situated at 1/2 span length and 1/4 chord length; (**b**) The intersection point positioned at 1/4 span length and 1/4 chord length.

For comparison, the elastic support stiffness coefficient is set to 1×10^6 N/m^2, and both m_1 and m_2 are assigned a value of 0.03 kg. The corresponding flutter speeds and frequencies for the configurations in Figure 8 are presented in Figures 9 and 10, respectively.

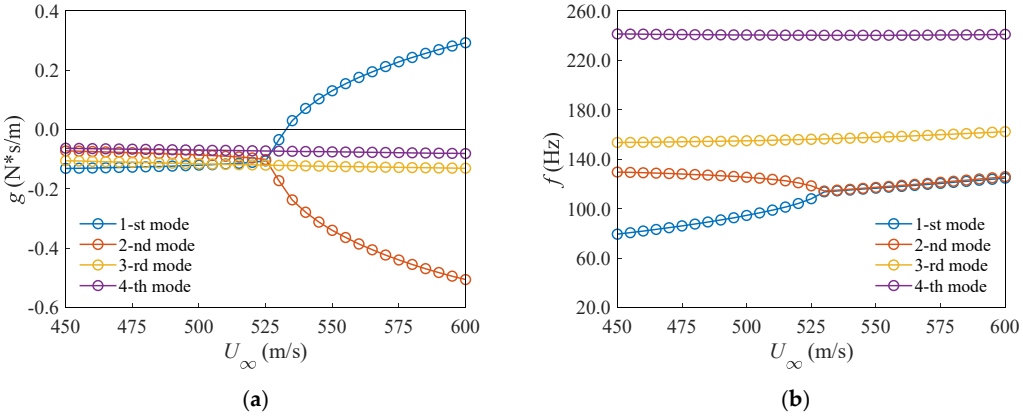
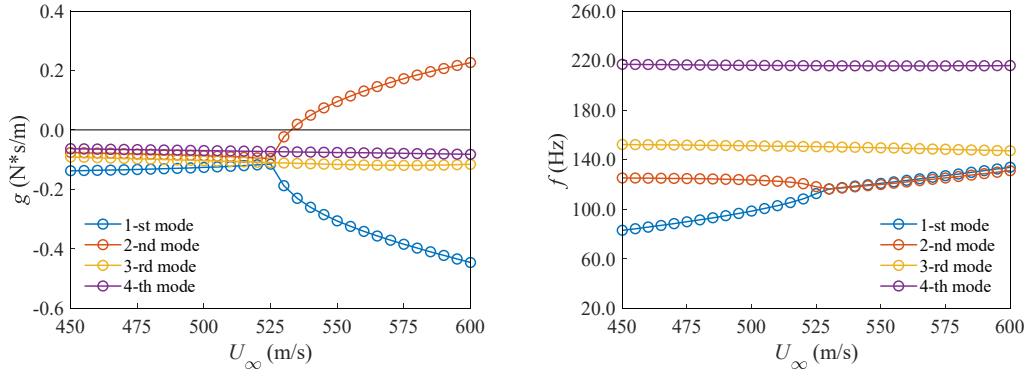


Figure 9. Flutter analysis results (LF-m_1): (**a**) $U - g$; (**b**) $U - f$.



(**a**) (**b**)

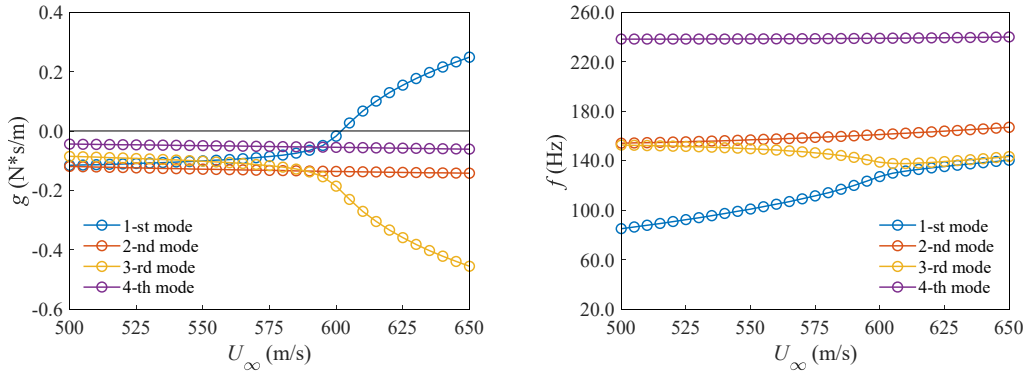
Figure 10. Flutter analysis results (LF-m_2): (**a**) $U-g$; (**b**) $U-f$.

As shown in Figure 9, for the case in Figure 8a, the panel exhibits a flutter speed of 532.67 m/s and a flutter frequency of 114.02 Hz. The corresponding suddenness factor is 0.0128, and flutter occurs in the first mode due to coupling between the first and second modes. Similarly, Figure 10 shows that for the configuration in Figure 8b, the panel's flutter speed is 532.74 m/s with a flutter frequency of 116.73 Hz. In this case, the suddenness factor is 0.0085, and flutter occurs in the second mode as a result of coupling with the first mode.

A comparison of Figures 6, 9 and 10 reveals that the position of the attached mass significantly influences the panel's flutter behaviors. While a centrally located mass increases the flutter speed relative to the baseline case without added mass, attaching the same mass at other positions—such as those in Figure 8—can lead to a notable reduction in flutter speed. This positional sensitivity suggests a potential strategy for dynamically regulating flutter boundaries: by integrating a movable mass component, the flutter characteristics of the panel may be adjusted within a certain range through controlled variation in the mass location.

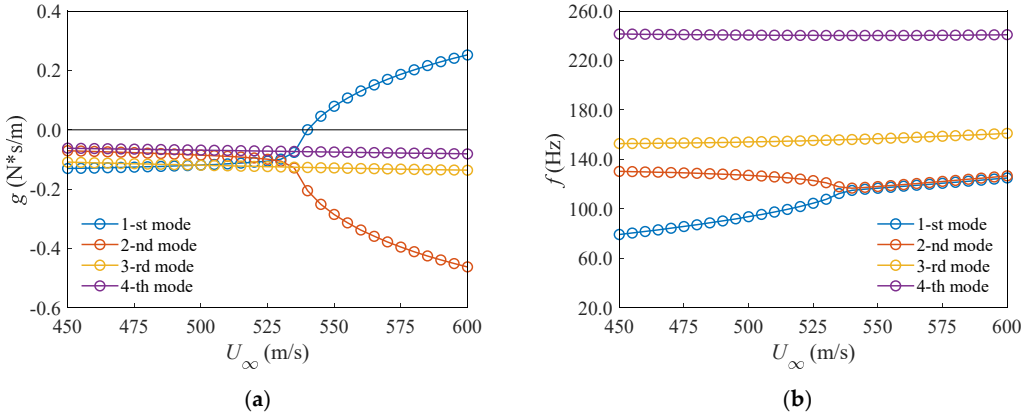
5.1.2. The Case of LB

This section examines the case where the leeward edge of the panel is elastically supported, with a uniform stiffness coefficient of 1×10^6 N/m^2. Three configurations are considered based on the mass attachment positions shown in Figures 6, 9 and 10, denoted as LB-m_c, LB-m_1, and LB-m_2, respectively. The corresponding flutter speeds and frequencies for these cases are presented in Figures 11–13.



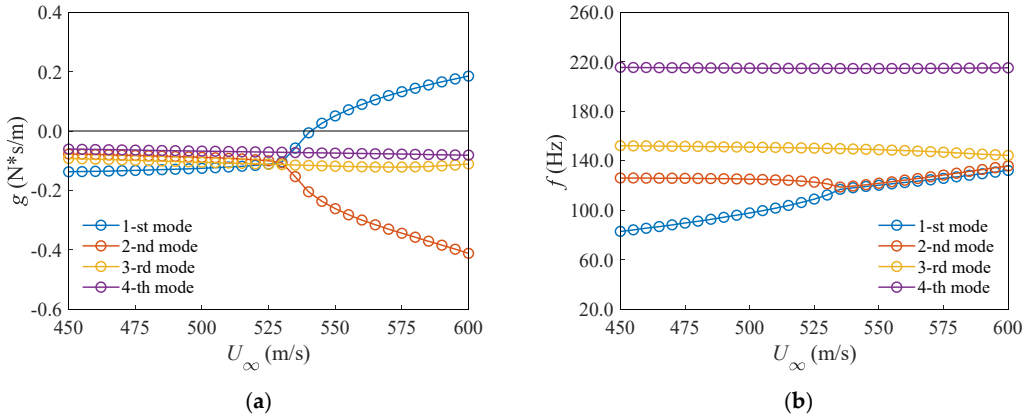
(**a**) (**b**)

Figure 11. Flutter analysis results (LB-m_c): (**a**) $U-g$; (**b**) $U-f$.



(**a**) (**b**)

Figure 12. Flutter analysis results (LB-m_1): (**a**) $U-g$; (**b**) $U-f$.



(**a**) (**b**)

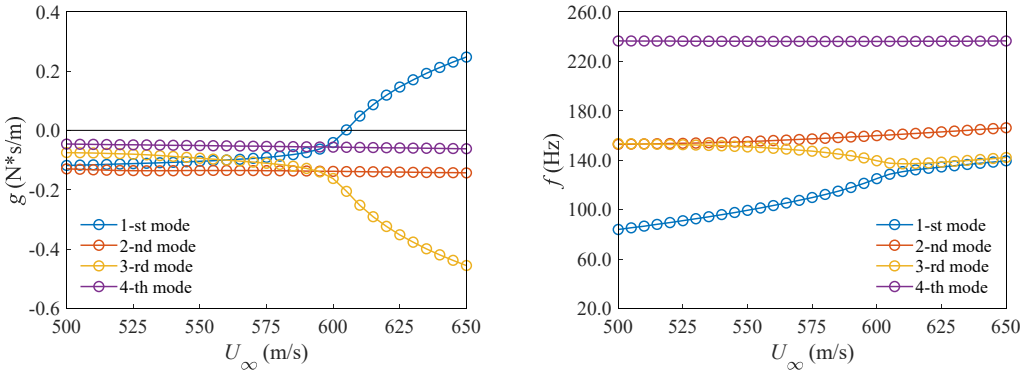
Figure 13. Flutter analysis results (LB-m_2): (**a**) $U-g$; (**b**) $U-f$.

As shown in Figures 11–13, the flutter speeds for the three configurations are 601.96 m/s, 539.99 m/s, and 540.91 m/s, with corresponding flutter frequencies of 128.23 Hz, 115.02 Hz, and 118.35 Hz, respectively. Analysis of these results indicates that when the leeward edge is elastically supported, attaching a mass at the panel center still effectively improves the flutter speed. In contrast, relocating the same mass to other positions leads to a noticeable reduction in both flutter speed and frequency. Furthermore, as observed in Figures 12 and 13, the flutter characteristics under these two non-central mass configurations show considerable similarity in both flutter speeds and frequencies.

5.1.3. The Case of LR/LT

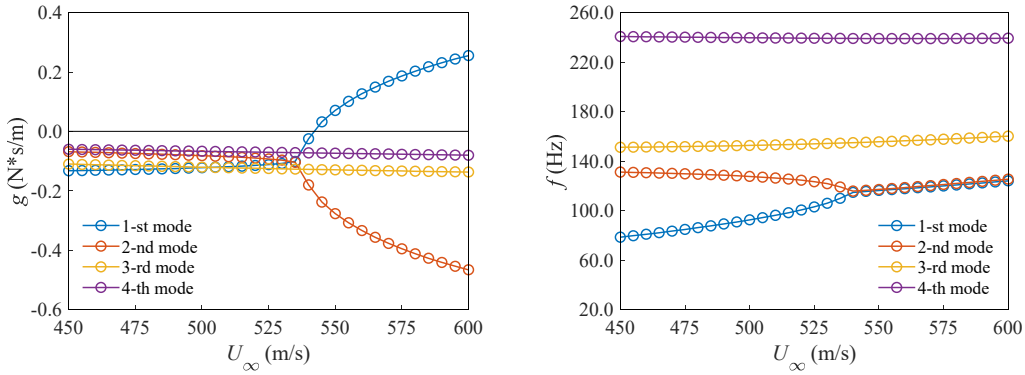
Following the approach in the above section, this section examines the case where the edge along the spanwise direction is elastically supported. Owing to the symmetry of the panel, the results for cases LR and LT are identical. Thus, the analysis is confined to case LR, with emphasis on how the flutter characteristics vary with the position of the attached mass. Three configurations are considered, denoted as LR-m_c, LR-m_1, and LR-m_2, respectively. The corresponding flutter speeds and frequencies for these sub-cases are provided in Figures 14–16.

As shown in these figures, the flutter speeds for the three configurations are 604.78 m/s, 542.16 m/s, and 536.71 m/s, with corresponding flutter frequencies of 128.42 Hz, 115.03 Hz, and 116.24 Hz, respectively.



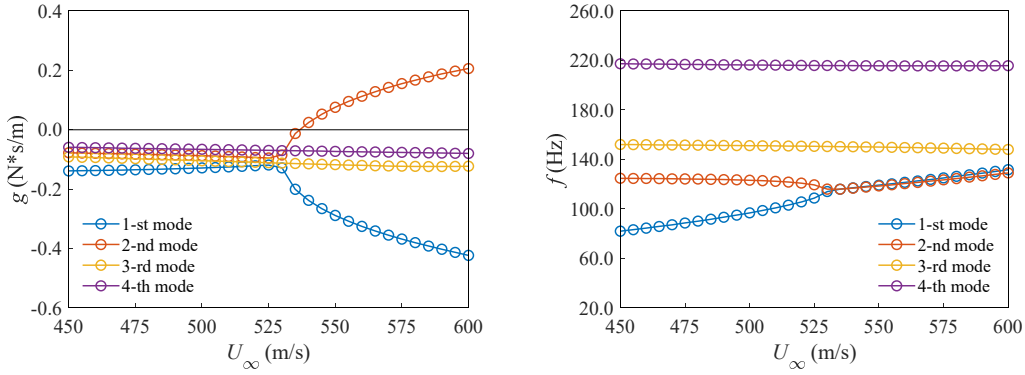
(**a**) (**b**)

Figure 14. Flutter analysis results (LR-m_c): (**a**) $U-g$; (**b**) $U-f$.



(**a**) (**b**)

Figure 15. Flutter analysis results (LR-m_1): (**a**) $U-g$; (**b**) $U-f$.



(**a**) (**b**)

Figure 16. Flutter analysis results (LR-m_2): (**a**) $U-g$; (**b**) $U-f$.

Furthermore, for clarity, the flutter characteristics of the panel under various working conditions are summarized in Table 3. And one can draw the following conclusions from the data in Table 3. First, compared to the baseline case without any mass attachment, attaching a mass at the center of the panel effectively increases the flutter speed, regardless of which edge is elastically supported. In contrast, when the mass is positioned elsewhere, the flutter speed may decrease sharply, in some cases falling below the original flutter speed of the panel. Second, the flutter frequencies of panels with attached masses are consistently lower than those of simply supported panels without mass attachments. It is worth noting, however, that when the mass is located at the panel center, the reduction in flutter frequency is less pronounced compared to other attachment locations. Third, based on the flutter slope data, placing a mass at the intersection of the 1/2 spanwise and 1/4 chordwise locations significantly increases the risk of a sudden onset of flutter. Finally, with regard to flutter modes, the

simply supported panel without mass attachment flutters in the 3rd mode. When a mass is attached at the center or at the 1/2 spanwise and 1/4 chordwise position, the flutter shifts to the 1st mode. In contrast, when the mass is placed at the 1/4 spanwise and 1/4 chordwise point, the panel is more likely to flutter in the 2nd mode.

Table 3. Flutter characteristics under different boundary support conditions.

Case	U_F (m/s)	f_F (Hz)	s_F	Mode	Couple Mode
NP	544.66	135.77	0.0108	3	1
LF-m_c	600.57	127.72	0.0089	1	3
LF-m_1	532.67	114.02	0.0128	1	2
LF-m_2	532.74	116.73	0.0085	2	1
LB-m_c	601.96	128.23	0.0089	1	3
LB-m_1	539.99	115.02	0.0153	1	2
LB-m_2	540.91	118.35	0.0064	1	2
LR-m_c	604.78	128.42	0.0085	1	3
LR-m_1	542.16	115.03	0.0114	1	2
LR-m_2	536.71	116.24	0.0075	2	1

5.2. Flutter Calculation of the Panel with Elastic Supports on All Four Sides

When all four sides of the panel are elastically supported, the configuration is denoted as FS. Based on the location of the mass attachment, this case is further divided into three sub-cases: FS-m_c, FS-m_1, and FS-m_2. With the elastic support stiffness coefficients maintained at 1×10^6 N/m^2, the corresponding flutter speeds and frequencies for these three configurations are presented in Figures 17–19, respectively.

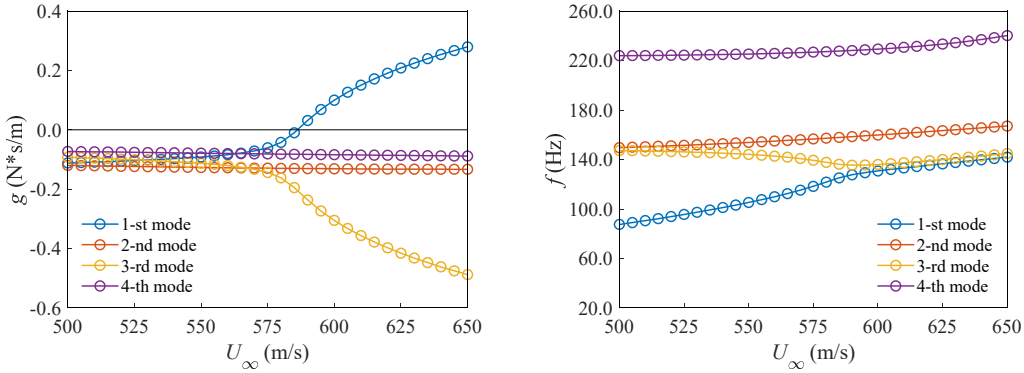


Figure 17. Flutter analysis results (FS-m_c): (**a**) $U-g$; (**b**) $U-f$.

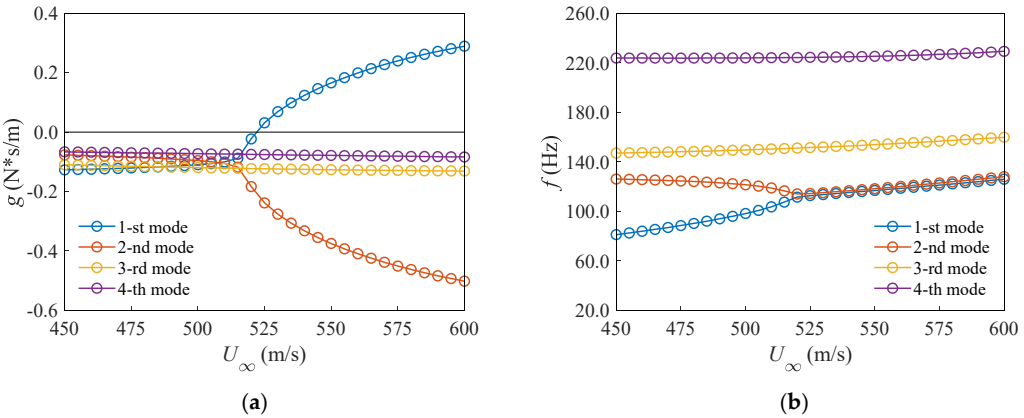


Figure 18. Flutter analysis results (FS-m_1): (**a**) $U-g$; (**b**) $U-f$.

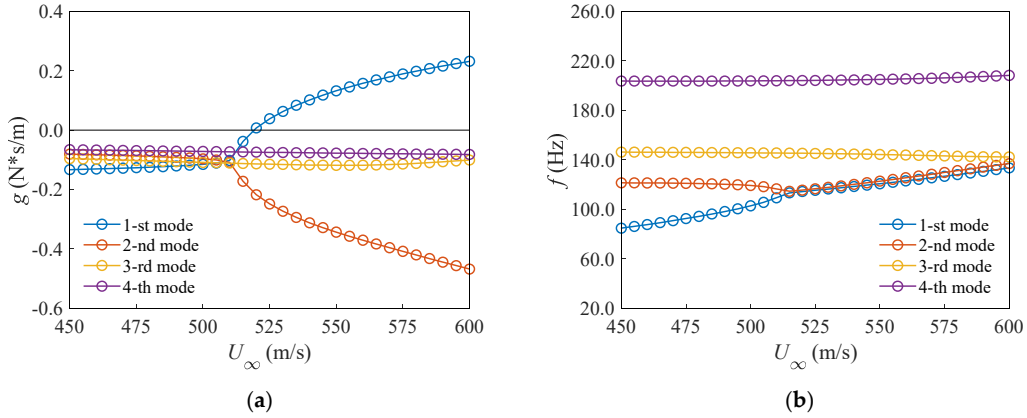


Figure 19. Flutter analysis results (FS-m_2): (**a**) $U-g$; (**b**) $U-f$.

As shown in these figures, the flutter speeds for configurations FS-m_c, FS-m_1, and FS-m_2 are 586.15 m/s, 522.11 m/s, and 519.22 m/s, respectively, with corresponding flutter frequencies of 125.78 Hz, 111.98 Hz, and 114.12 Hz. A comparison with the data in Table 3 reveals that as the number of elastically supported edges increases, both the flutter speed and frequency decrease to varying degrees under identical mass attachment conditions. Nevertheless, the influence of mass location on the flutter characteristics remains consistent with that observed in the single-edge elastic support cases.

To more clearly observe the variation patterns of the flutter characteristics of the panel with the stiffness coefficient of the elastic support, the variation laws of the flutter speed, flutter frequency, flutter slope and flutter mode with respect to the stiffness coefficient of the elastic supports and the mass of the attachment are plotted in Figure 20. It is noteworthy that the attachment position of the mass component is at the intersection of 1/4 spanwise and 1/4 chordwise.

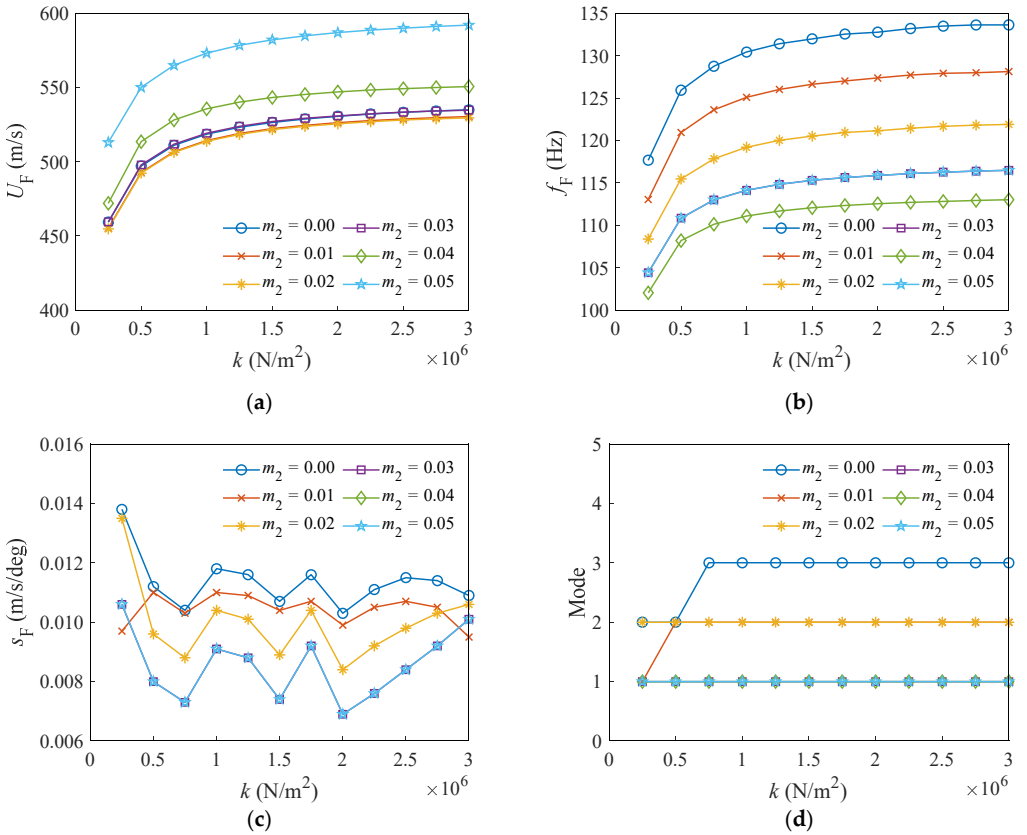


Figure 20. Flutter characteristics vs. the stiffness coefficient of the elastic support for different mass (FS-m_2): (**a**) Flutter speeds; (**b**) flutter frequencies; (**c**) Flutter slopes; (**d**) flutter modes.

As can be seen from Figure 20a, when the mass of the attachment is relatively small, the flutter speed curves are dense. As the mass of the attachment increases continuously, the increase in flutter speed becomes more pronounced. In contrast, Figure 20b shows that the flutter frequency curves begin to converge when the mass of the attachment is large, but the degree of density is not as significant as that of flutter speeds. Similarly, both flutter speeds and flutter frequencies exhibit a monotonic increasing trend with the increase in the stiffness coefficients of the elastic supports. According to Figure 20c, the suddenness of the panel entering the flutter state does not decrease significantly with the increase in the stiffness coefficients of the elastic supports. However, it decreases markedly with the increase in the attached mass. Finally, Figure 20d reveals that when there is no attachment or the mass of the attachment is small, the flutter mode of the panel is primarily the second or third mode. As the mass of the attachment continues to increase, the flutter mode of the panel entering the flutter state primarily manifests as the first mode.

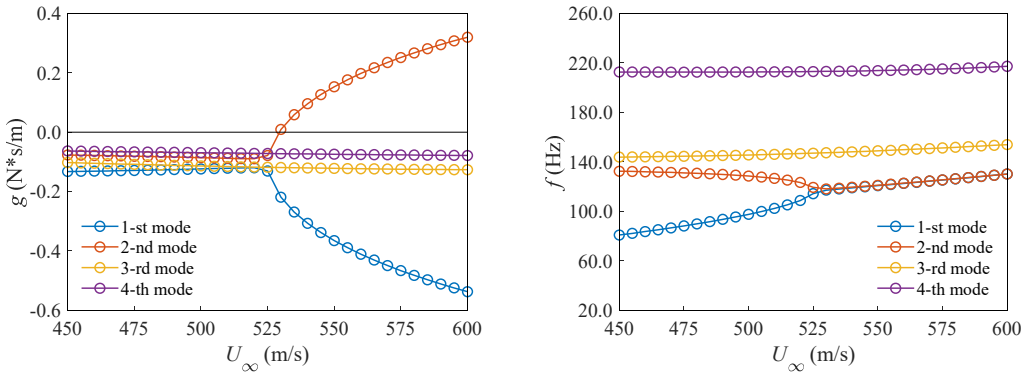
5.3. Flutter Calculation of the Panel with Multiple Mass Attachments

In practical applications, panels may be subjected to multiple attached masses. Two typical scenarios are investigated here: one with a larger mass concentrated at the panel center, and another with masses distributed away from the center. The following configurations are examined:

(1) Case FS-m_E: Mass attachments are located at the panel center, the 1/2 spanwise and 1/4 chordwise intersection, and the 1/4 spanwise and 1/4 chordwise intersection, with masses m_c = 0.01 kg, m_1 = 0.01 kg, and m_2 = 0.01 kg, respectively.

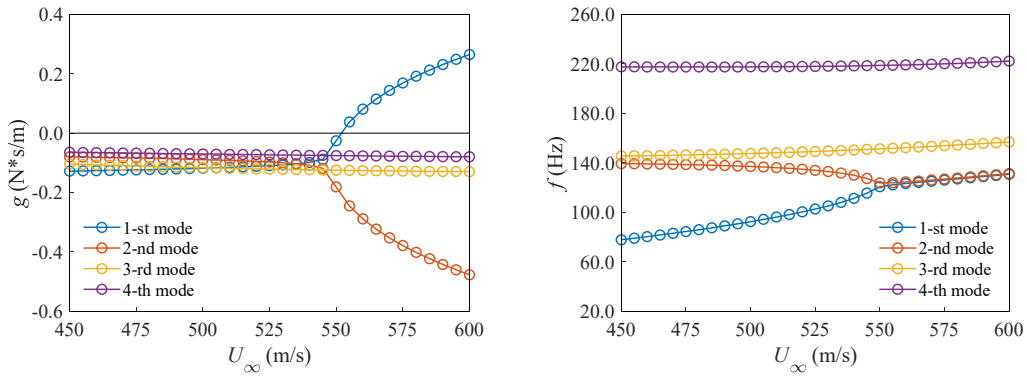
(2) Case FS-m_U: Masses are placed at the same positions as in FS-m_E, but with redistributed values: m_c = 0.02kg, m_1 = 0.005 kg, and m_2 = 0.005 kg.

The flutter speed and frequency curves for these two cases are shown in Figures 21 and 22, respectively. For Case FS-m_E (Figure 21), the flutter speed and frequency are 529.48 m/s and 118.25 Hz, respectively. In contrast, Case FS-m_U (Figure 22) exhibits a flutter speed of 552.01 m/s and a frequency of 121.37 Hz.



(**a**) (**b**)

Figure 21. Flutter analysis results (FS-m_E): (**a**) $U-g$; (**b**) $U-f$.



(**a**) (**b**)

Figure 22. Flutter analysis results (FS-m_U): (**a**) $U-g$; (**b**) $U-f$.

These results clearly demonstrate that the spatial distribution of attached masses significantly influences the flutter characteristics of elastically supported panels. Concentrating mass near the panel center leads to higher flutter speeds, whereas distributing mass toward peripheral regions results in a noticeable reduction in flutter performance.

Furthermore, the variations in flutter speed and frequency are closely related to the frequency gap between the participating modes. Generally, a smaller frequency gap facilitates earlier mode coupling and thus earlier flutter onset, while a larger gap delays it. In this study, the central mass m_c increases the frequency separation between the first and second modes, which postpones mode coupling and raises the flutter speed. The off-center masses m_1 and m_2 reduce the frequency gap between the lower-order modes, promoting earlier modal interaction and leading to a decrease in flutter speed. A reduction in elastic support stiffness (simulating damage) significantly lowers the natural frequencies of the lower-order modes, thereby narrowing the frequency gap with higher-order modes and accelerating the onset of flutter. This mechanism provides a frequency-domain explanation for the flutter-boundary trends observed in Sections 5.1–5.3.

5.4. Flutter Characteristics of the Panel with Dampers

The analysis in Sections 5.1–5.3 demonstrates that the flutter characteristics of the panel—especially the flutter speed—are influenced by multiple factors, including the stiffness and location of elastic supports, as well as the mass and distribution of attached objects. However, the flutter boundary of the panel is typically determined during the design phase. Any subsequent changes in support conditions or added masses during service may alter the panel's dynamic properties, thereby affecting its flutter speed and frequency. A significant reduction in flutter speed poses considerable risks to both structural integrity and flight safety. It is therefore essential to develop strategies that preserve or even enhance the flutter performance of the panel after design finalization, even in the presence of modified supports or added masses.

As expressed in Equation (27), the introduction of damping can significantly influence the solution of the eigenvalue problem. Structural damping continuously dissipates energy from the self-excited vibration of the panel, requiring a higher flow speed to maintain simple harmonic motion. It is thus effective to position dampers at locations with high vibration velocity. Based on the modal characteristics of a simply supported panel without mass attachments, two damper configurations are proposed in this study: the 5P method and the 9P method, as illustrated in Figure 23.

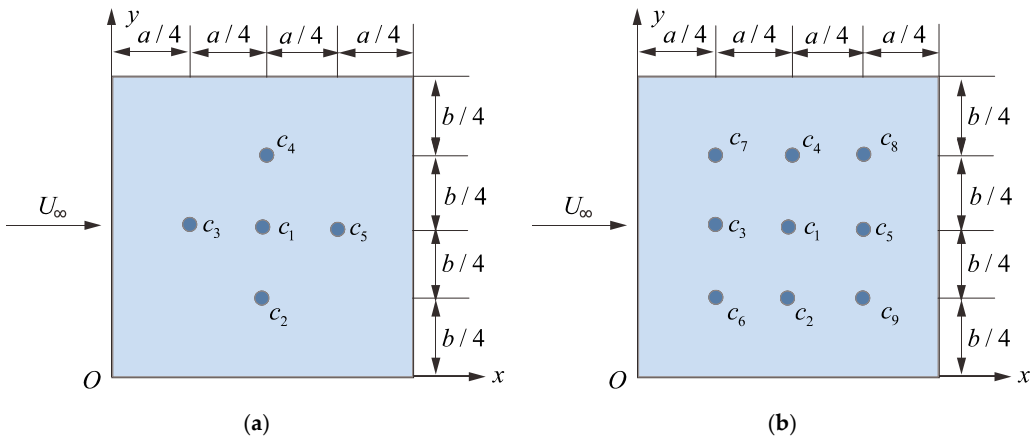
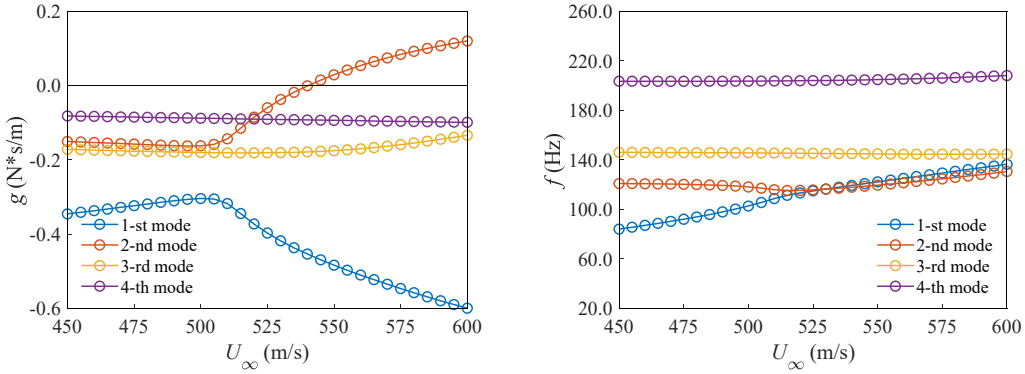


Figure 23. Two distinct damper arrangements for mitigating panel flutter: (**a**) the 5P method; (**b**) the 9P method.

The 5P and 9P damper configurations are designed based on the modal characteristics of the baseline simply supported panel, with dampers positioned at the anti-nodes of the first few bending modes to maximize energy dissipation.

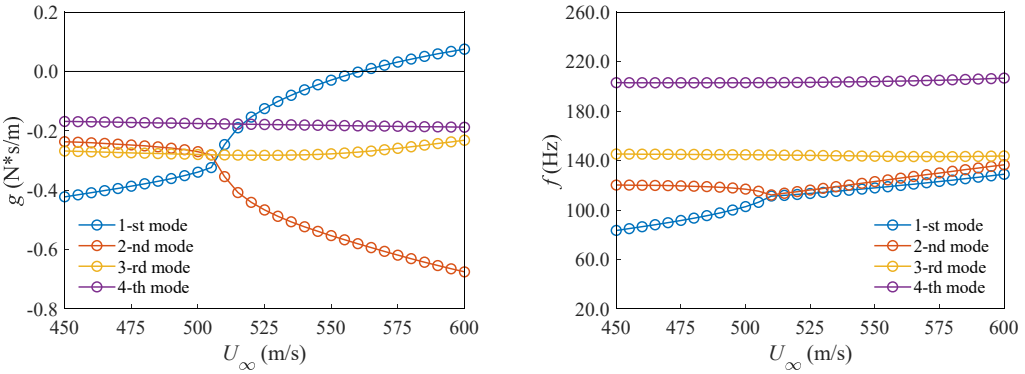
The FS-m_2 configuration is used to demonstrate the improvement in flutter characteristics achievable through the application of dampers. This study considers a simplified scenario in which all pre-installed dampers have identical damping coefficients.

First, with the damping coefficient set to $c = 3.0$, the flutter speeds and frequencies of the panel under the FS-m_2 case are computed for the 5P and 9P damper configurations, as shown in Figures 24 and 25, respectively. As observed in Figure 24, the 5P method yields a flutter speed of 540.21 m/s and a flutter frequency of 117.84 Hz. However, as shown in Figure 25, the panel exhibits a flutter speed of 560.88 m/s and a flutter frequency of 120.05 Hz when dampers are applied. Compared to the undamped case FS-m_2 (flutter speed 519.22 m/s, frequency 114.12 Hz) and the baseline case NP (flutter speed 544.66 m/s, frequency 135.77 Hz), the 5P configuration with a damping coefficient of 3.0 increases the flutter speed by approximately 21 m/s, bringing it close to the value targeted during the initial design phase. Further improvement can be achieved using the 9P method, which raises the flutter speed by about 2.98% relative to the 5P method.



(**a**) (**b**)

Figure 24. Flutter analysis results (FS-m_2-5P): (**a**) $U - g$; (**b**) $U - f$.



(**a**) (**b**)

Figure 25. Flutter analysis results (FS-m_2-9P): (**a**) $U - g$; (**b**) $U - f$.

A comparison of the flutter frequency curves in Figures 24b and 25b reveals nearly identical results between the 5P and 9P methods. Additionally, Figures 24 and 25 highlight a noteworthy phenomenon: when structural damping is introduced, the flutter point no longer coincides with the mode coupling point. For example, in Figure 25, the flutter speed is 560.88 m/s, whereas the first and second modes begin to couple at a flow velocity of approximately 510 m/s.

To gain a deeper insight into the benefits of the configured dampers, the case FS-m_2 is again utilized as an example. By adjusting the damping coefficient within the range of 0 to 5 N×s/m, the variations in the flutter speeds and frequencies can be observed, as illustrated in Figure 26. It can be observed from Figure 26 that both the 5P method and the 9P method are effective. The flutter characteristics according to the 5P method exhibit a linear increase with the damping coefficient. However, the flutter speeds and frequencies of the panel based on the 9P method increase at a faster rate, demonstrating a trend of nonlinear growth. Specifically, when c reaches 5, the flutter speed and flutter frequency, as determined by the 9P method, are 612.80 m/s and 129.25 Hz, respectively. In comparison to the case FS-m_2 without dampers, the panel's flutter speed and frequency exhibit an increase of 18.02% and 13.26%, respectively.

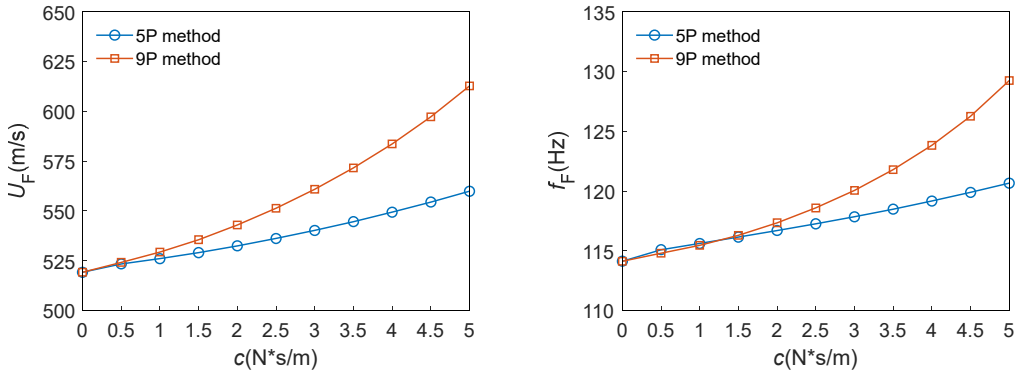


Figure 26. The impact of the two damping configurations on the flutter behavior of the panel: (**a**) $U_F - c$; (**b**) $f_F - c$.

To further evaluate the performance of the proposed damper configurations, the FS-m_2 case is revisited. By varying the damping coefficient between 0 and 5 N·s/m, the corresponding variations in flutter speed and frequency are obtained, as shown in Figure 26. The results demonstrate the effectiveness of both the 5P and 9P configurations. The flutter characteristics of the 5P configuration increase approximately linearly with the damping coefficient. In contrast, the 9P configuration exhibits a nonlinear growth trend, with both flutter speed and frequency rising at a significantly faster rate. Specifically, at a damping coefficient of $c = 5$, the 9P method achieves a flutter speed of 612.80 m/s and a flutter frequency of 129.25 Hz. Compared to the undamped FS-m_2 case, this represents an improvement of 18.02% in flutter speed and 13.26% in flutter frequency. Figure 26 demonstrates that the flutter speed increases monotonically with the damping coefficient, confirming the effectiveness of added damping. A full optimization balancing damping performance with other constraints (e.g., added mass, volume) is a subject for future detailed design studies. The present focus on panels with elastic supports directly addresses the predominant failure mechanism of stiffness degradation in thin-walled aircraft structures, which accounts for a majority of in-service failures [1]. The proposed damper configurations provide a viable pathway to recover lost flutter performance in such compromised panels.

6. Conclusions

This study establishes a structural dynamics model for supersonic panels with elastic (damaged) supports and attached masses using a novel two-stage assumed mode method. By integrating first-order piston theory aerodynamics and solving the resulting aeroelastic equations with the p-k method, the flutter characteristics are systematically investigated under a wide range of support stiffness, mass, and damper configurations. The key quantitative findings and conclusions are summarized as follows:

(1) The proposed two-stage assumed mode method accurately captures the modal properties of panels with elastic supports and discrete mass attachments. For a panel with a single elastically supported edge, a centrally attached mass of 0.03 kg (≈10% of the panel mass) increases the flutter speed by approximately 10% while reducing the flutter frequency by about 6%, compared to the simply supported baseline without mass. In contrast, placing the same mass at off-center locations (e.g., at 1/4 chord) can reduce the flutter speed by roughly 2–4%. This strong positional sensitivity highlights the potential for actively tuning flutter behavior using a movable mass element.

(2) Increasing the number of elastically supported edges consistently lowers both the flutter speed and frequency under identical mass attachment conditions. The degradation is most pronounced when all four sides are elastic, where the flutter speed for an off-center mass case can drop by more than 4% relative to the single-edge elastic support configuration. Nevertheless, the qualitative influence of mass location remains consistent across different support scenarios.

(3) The spatial distribution of attached masses considerably affects the flutter performance. Concentrating mass near the panel center improves the flutter boundary, whereas a dispersed

arrangement leads to noticeable degradation. This underlines the importance of considering mass distribution in the design and assessment of panel-like components.

(4) The flutter characteristics of panels with compromised supports and added masses can be substantially recovered and even enhanced through optimized damper placement. Both the 5P and 9P damper layouts improve the flutter speed and frequency, with the 9P configuration showing superior performance. For instance, with a damping coefficient of 5 N·s/m, the 9P layout increases the flutter speed by up to 18% and the flutter frequency by over 13% for a panel with four-sided elastic supports and an off-center mass, thereby exceeding the original design flutter boundary.

In summary, the present work provides a realistic and efficient analytical framework for simulating the in-service dynamics of panels subject to combined boundary flexibility and discrete mass attachments. The findings offer concrete, quantitative insights for the design, diagnosis, and mitigation of flutter in aerospace panel structures, contributing to enhanced flight safety under complex operational conditions. While this study demonstrates the aeroelastic feasibility and potential of the proposed approach, its practical implementation would require further design integration studies to address associated challenges such as added weight, system integration, and maintenance.

Author Contributions: Conceptualization, W.Q. and S.T.; methodology, W.Q.; software, S.Y.; validation, S.Y.; formal analysis, S.T.; investigation, S.Y.; resources, S.T.; data curation, S.T.; writing—original draft preparation, S.T.; writing—review and editing, W.Q.; visualization, S.Y.; supervision, S.T.; project administration, W.Q.; funding acquisition, W.Q. All authors have read and agreed to the published version of the manuscript.

Funding: This research was funded by the National Natural Science Foundation of Liaoning (grant numbers 2025-MSLH-565) and the Project of Liaoning Provincial Department of Education (grant numbers JYTMS20230253, JYTMS20230224).

Data Availability Statement: The original contributions presented in this study are included in the article. Further inquiries can be directed to the corresponding author.

Conflicts of Interest: The authors declare no conflicts of interest.

References

1. Ren, R.; Ma, X.Y.; Yue, H.H.; Yang, F.; Lu, Y.F. Stiffness enhancement methods for thin-walled aircraft structures: A review. *Thin Wall Struct.* **2024**, *201*, 111995. [CrossRef]
2. Zhou, Y.S.; Wang, Q.S.; Shi, D.Y.; Liang, Q.; Zhang, Z.Y. Exact solutions for the free in-plane vibrations of rectangular plates with arbitrary boundary conditions. *Int. J. Mech. Sci.* **2017**, *130*, 1–10. [CrossRef]
3. Zhou, K.; Huang, X.C.; Zhang, Z.G.; Hua, H.X. Aero-thermo-elastic flutter analysis of coupled plate structures in supersonic flow with general boundary conditions. *J. Sound Vib.* **2018**, *430*, 36–58. [CrossRef]
4. Zhou, K.; Huang, X.C.; Tian, J.J.; Hua, H.X. Vibration and flutter analysis of supersonic porous functionally graded material plates with temperature gradient and resting on elastic foundation. *Compos. Struct.* **2018**, *204*, 63–79. [CrossRef]
5. Zhou, K.; Hu, Z.M.; Hua, H.X. Investigations on the aero-thermo-elastic characteristics of arbitrary polygon built-up structures in supersonic airflow. *Int. J. Mech. Sci.* **2021**, *196*, 106300. [CrossRef]
6. Lin, H.G.; Cao, D.Q.; Xu, Y.Q. Vibration characteristics and flutter analysis of a composite laminated plate with a store. *Appl. Math. Mech. Engl. Ed.* **2018**, *39*, 241–260. [CrossRef]
7. Su, Z.; Wang, L.F.; Sun, K.P.; Wang, D. Vibration characteristic and flutter analysis of elastically restrained stiffened functionally graded plates in thermal environment. *Int. J. Mech. Sci.* **2019**, *157–158*, 872–884. [CrossRef]
8. Tian, S.M.; Wang, M.; Qi, W.C. Effects of elastically supported boundaries on flutter characteristics of thin-walled panels. *Energies* **2022**, *15*, 7088. [CrossRef]
9. Baghaee, M.; Farrokhabadi, A.; Jafari-Talookolaei, R.A. Modeling, analysis, and control of MFC sandwiched laminate panel flutter with general layups and arbitrary boundary conditions. *Compos. Struct.* **2019**, *223*, 110940. [CrossRef]
10. Algazin, S.D. Flutter of an arbitrary shaped plate with mixed boundary conditions in a plane. *Mech. Solids* **2022**, *57*, 128–131. [CrossRef]
11. Jin, Y.Q.; Luo, X.W.; Liu, H.X.; Qiu, B.S.; Chi, H.Y. An accurate solution method for vibration analysis of multi-span lattice sandwich beams under arbitrary boundary conditions. *Thin Wall. Struct.* **2022**, *175*, 109214. [CrossRef]
12. Xie, K.; Xu, K.; Dong, W.J.; Chen, M.X. An analytic method for vibration analysis of non-uniformly coupled L-shaped plates with arbitrary boundary conditions. *Thin Wall. Struct.* **2023**, *18*, 110639. [CrossRef]

13. Sun, Q.Z.; Xing, Y.F.; Liu, B.; Zhang, B.C.; Wang, Z.K. Accurate closed-form eigensolutions of three-dimensional panel flutter with arbitrary homogeneous boundary conditions. *Chin. J. Aeronaut.* **2023**, *36*, 266–289. [CrossRef]
14. Fazelzadeh, S.A.; Mazidi, A.; Kalantari, H. Bending-torsional flutter of wings with an attached mass subjected to a follower force. *J. Sound Vib.* **2009**, *323*, 148–162. [CrossRef]
15. Fazelzadeh, S.A.; Kazemi-Lari, M.A. Stability analysis of a partially loaded leipholz column carrying a lumped mass and resting on elastic foundation. *J. Sound Vib.* **2013**, *332*, 595–607. [CrossRef]
16. Peiro', J.; Galvanetto, U.; Chantharasenawong, C. Assessment of added mass effects on flutter boundaries using the Leishman–Beddoes dynamic stall model. *J. Fluid. Struct.* **2010**, *26*, 814–840. [CrossRef]
17. Wang, Y.R.; Liang, T.W. Application of lumped-mass vibration absorber on the vibration reduction of a nonlinear beam-spring-mass system with internal resonances. *J. Sound Vib.* **2015**, *350*, 140–170. [CrossRef]
18. Aydogdu, M.; Filiz, S. Vibration analysis of symmetric laminated composite plates with attached mass. *Mech. Adv. Mater. Struct.* **2016**, *23*, 136–145. [CrossRef]
19. Rahmane, A.; Benmansour, T.; Bouakba, M.; Mdedour, I. Factors influencing the effect of attached mass on dynamic behavior of laminate composite plates using Taguchi technique. *J. Braz. Soc. Mech. Sci.* **2018**, *40*, 66. [CrossRef]
20. Amoozgar, M.R.; Shaw, A.D.; Zhang, J.; Friswell, M.I. The effect of a movable mass on the aeroelastic stability of composite hingeless rotor blades in hover. *J. Fluid Struct.* **2019**, *87*, 124–136. [CrossRef]
21. Sun, Y.H.; Song, Z.G.; Ma, W.S.; Li, F.M. Influence mechanism of lumped masses on the flutter behavior of structures. *Aerosp. Sci. Technol.* **2021**, *111*, 106524. [CrossRef]
22. Qi, W.C.; Wang, M.; Tian, S.M. Effects of mass attachments on flutter characteristics of thin-walled panels. *Aerospace* **2022**, *9*, 748. [CrossRef]
23. Uymaz, B. Vibration of CFFF functionally graded plates with an attached point mass at an arbitrary point in thermal environment. *J. Vib. Eng. Technol.* **2022**, *11*, 1867–1888. [CrossRef]
24. Zhang, Z.G.; Ji, H.L.; Tao, C.C.; Qiu, J.H.; Cheng, L. Suppression of panel flutter in supersonic flow based on acoustic black hole as a linear energy sink. *J. Sound Vib.* **2024**, *571*, 118030. [CrossRef]
25. Najafi, M.; Ferreira, A.J.M.; Marques, F.D. Aeroelastic analysis of a lightweight topology-optimized sandwich panel. *Proc. Inst. Mech. Eng. Part G J. Aerosp. Eng.* **2024**, *238*, 999–1017. [CrossRef]
26. Liu, T.; Bu, G.Z.; Wang, J.F.; Zheng, Y.; Li, Y.F. Determination of critical aerodynamic pressure in flutter analysis of a novel three-phase composite trapezoidal plate under supersonic flow. *Eng. Struct.* **2026**, *346B*, 121677. [CrossRef]
27. Zhao, Y.H.; Huang, R. *Advanced Aeroelasticity and Control*; Science Press: Beijing, China, 2015; pp. 98–125, ISBN 978-7-03-044222-2.

Disclaimer/Publisher's Note: The statements, opinions and data contained in all publications are solely those of the individual author(s) and contributor(s) and not of MDPI and/or the editor(s). MDPI and/or the editor(s) disclaim responsibility for any injury to people or property resulting from any ideas, methods, instructions or products referred to in the content.